Chemistry–A European Journal
Research Article
doi.org/10.1002/chem.202301901
Chemistry Europe
European Chemical Societies Publishing
www.chemeurj.org

Tailoring Secondary Coordination Sphere Effects in Single-metal-site Catalysts by Surface Immobilization of Supramolecular Cages

Petrus C. M. Laan,[a] Eduard O. Bobylev,[a] Felix J. de Zwart,[a] Joppe A. Vleer,[a] Alessandro Troglia,[b] Roland Bliem,[b] Gadi Rothenberg,*[a] Joost N. H. Reek,*[a] and Ning Yan*[a, c]

Controlling the coordination sphere of heterogeneous single-metal-site catalysts is a powerful strategy for fine-tuning their catalytic properties but is fairly difficult to achieve. To address this problem, we immobilized supramolecular cages where the primary- and secondary coordination sphere are controlled by ligand design. The kinetics of these catalysts were studied in a model reaction, the hydrolysis of ammonia borane, over a temperature range using fast and precise online measurements generating high-precision Arrhenius plots. The results show how catalytic properties can be enhanced by placing a well-defined reaction pocket around the active site. Our fine-tuning yielded a catalyst with such performance that the reaction kinetics are diffusion-controlled rather than chemically controlled.

Introduction

The transition to sustainable energy involves new chemistries, that often require new tailor-made catalysts. An important development in this area are heterogeneous single-metal-site catalysts in which the active metal is atomically dispersed over the support and stabilized by neighbouring groups.[1,2] These catalysts provide 100% atom utilization, and often show exceptional reactivity thanks to their unique reactant-support interactions. Most of these materials are synthesized by impregnating a molecular precursor on the surface followed by thermal ligand removal. This prevents interference from the precursor ligands and forms new, strong metal-support bonds.[3] The surrounding support atoms form the first-coordination sphere, controlling the catalytic properties just like a ligand in an organometallic complex.[4,5]

Enzymes have, next to a well-defined active site, also a well-defined secondary coordination sphere, which is often crucial to the catalysts properties as it enhances substrate selectivity, substrate pre-activation and transition-state stabilization. Creating such a tailored secondary coordination sphere around supported single-metal-site catalysts is a major design and synthetic challenge.

One way to address this challenge is by using supramolecular coordination cages, where the cavity acts as the second coordination sphere.[6–8] Here we present a selective synthesis of supported single-metal-site catalysts with well-defined primary and secondary coordination spheres by immobilizing different supramolecular complexes containing Pt-N_4 metal nodes that can act as active site. First, we show that our method results in a homogenous distribution of the molecular species, and that the pre-organization of metal atoms is retained upon immobilization. Then, we evaluate these catalysts in the hydrolysis of ammonia borane using high-precision kinetic studies. We show how fine-tuning of the secondary coordination sphere can increase the reaction rates and lower activation barriers. Finally, we design and validate a solid catalyst of which the rate primarily depends on substrate diffusion and orientation, rather than on the reaction at the active site itself.

[a] P. C. M. Laan, Dr. E. O. Bobylev, F. J. de Zwart, J. A. Vleer, Prof. Dr. G. Rothenberg, Prof. Dr. J. N. H. Reek, Prof. Dr. N. Yan
Van 't Hoff Institute for Molecular Sciences
University of Amsterdam
Science Park 904, 1098 XH Amsterdam (The Netherlands)
E-mail: g.rothenberg@uva.nl
j.n.h.reek@uva.nl

[b] A. Troglia, Dr. R. Bliem
Advanced Research Center for Nanolithography (ARCNL)
Science Park 106, 1098XG Amsterdam (The Netherlands)

[c] Prof. Dr. N. Yan
Key Laboratory of Artificial Micro- and Nano-Structures of Ministry of Education, School of Physics and Technology
Wuhan University
Wuhan, 430072 (China)
E-mail: ning.yan@whu.edu.cn

Supporting information for this article is available on the WWW under https://doi.org/10.1002/chem.202301901

Results and Discussion

Design and synthesis of the model catalyst system

To study how second coordination sphere effects can influence reaction kinetics, we prepared a set of three model catalysts: **Pt_1**, **Pt_2** and **Pt_2'** (Figure 1).

We chose platinum-based complexes over their palladium analogues because of their higher kinetic stability.[9] Mononuclear **Pt_1** serves as a control catalyst as it has no cage as second coordination sphere, in contrast to **Pt_2**, which has an inner cavity that allows confinement effects to contribute to the catalytic performance (*vide supra*). The difference between **Pt_2** and **Pt_2'** is the presence of pyridine functionalities within the ligand scaffold providing basic groups in the second coordination sphere.

The three complexes were prepared according to published procedures and characterization by ^{1}H-NMR, 2D ^{1}H-DOSY-NMR, ^{13}C-NMR and HR-ESI-MS was in excellent agreement with literature (see details in supporting information, Figures S1–S15).[10,11] The ^{1}H-NMR spectra show typical downfield shifts of the pyridine proton signals upon coordination to platinum. The 2D ^{1}H-DOSY NMR spectra revealed that all proton signals of the formed species have an identical diffusion constant which is higher compared to the free ligands, indicating the formation of a larger species. The correct stoichiometry between ligand and metal was confirmed by HR-ESI-MS. The exact configurations of **Pt_1** and **Pt_2'** were confirmed by single crystal X-ray diffraction and compared to the known X-ray structure of **Pt_2** (Figures S16–S18).[11] We see minor (<0.02 Å) variations in Pt–N bond lengths, implying a similar electronic structure of the platinum nodes. This agrees with the XPS data of the pure complexes which have almost equal platinum binding energies (*vide infra*). Furthermore, the orientation of the bound pyridine rings (the first coordination sphere) was highly similar for all three catalysts based on an overlay of their X-ray structures (Figure S18). These similarities in the platinum environment of all three complexes ensure a similar reactivity of the platinum nodes. Any difference between the catalysts can therefore be attributed to second coordination sphere effects.

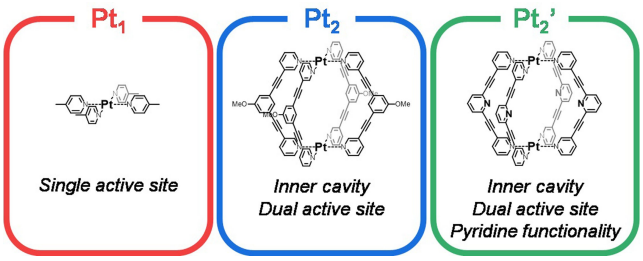

Figure 1. Molecular structures of model catalysts **Pt_1**, **Pt_2** and **Pt_2'**.

Immobilizing and characterising the complexes

With the pure molecular species at hand, we proceeded with surface immobilization on the chemically inert carbon support Vulcan. We used a conventional wet impregnation method to synthesize **Pt_1**@Vulcan, **Pt_2**@Vulcan and **Pt_2'**@Vulcan (see supporting information for details). The total platinum loading of each catalyst was kept equal to 0.1 wt%, which was confirmed by ICP-OES (Table S1). Moreover, the powder X-ray diffraction patterns after immobilization show only pure Vulcan while all three molecular precursors are highly crystalline (Figures S19–S21).[12] This suggests that the organometallic species are well dispersed over the support. Quantitative desorption of the molecular species followed by UV-Vis and HR-ESI-MS analysis indicate that the molecular species stay intact upon immobilization (Figures S22–S27 and Table S2).

Next, we ran aberration-corrected HAADF-STEM measurements to study the dispersion and structure of the catalysts (Figure 2 and Figures S28–S29).

The Ångstrom resolution images show single bright dots on the carbon support with a diameter close to that of a platinum atom (0.177 nm) as determined by intensity profiling (Figure S28).[13] This indicates that immobilization of **Pt_1** on Vulcan results in the formation of atomically dispersed platinum atoms without any cluster or nanoparticle formation. Moreover, the corresponding EDX elemental mapping also supports the homogenous and atomic distribution of **Pt_1**. By contrast, surface immobilization of **Pt_2'** showed only *pairs* of platinum atoms, in line with immobilization of molecular cage complexes that remains intact (Figure 2). Here, too, the diameter of the bright dot matches that of a platinum atom (Figure S29) and the molecular cages **Pt_2'** did not show agglomeration during immobilization. The distribution in metal-to-metal distances reflects the various orientations of the spherical **Pt_2'** structure on the support. The fact that the precursors did not agglomerate is important for a fair comparison of the catalytic performance, as all the metal atoms are accessible for catalysis in our case.

Additionally, the samples were analysed by XPS to study possible electronic effects upon immobilization (Figures S30–S32). The spectra before and after immobilization of the Pt 4f core levels were dominated by one species, consistent with a single type of platinum for each sample. Upon immobilization, the core-level binding energies showed only minor (<0.4 eV) shifts. This confirms that in addition to the equal distribution of the molecular species, there is no change in the electronic properties of the platinum nodes.

Catalytic hydrolysis of ammonia borane

Subsequently, we studied the three catalysts in the hydrolysis of ammonia borane (Eq. 1) in water at ambient pressure between 15 and 80 °C (Figure 3 and Figures S33–S39).

$$NH_3BH_3 + 4H_2O \rightarrow NH_4^+ + B(OH)_4^- + 3H_2 \quad (1)$$

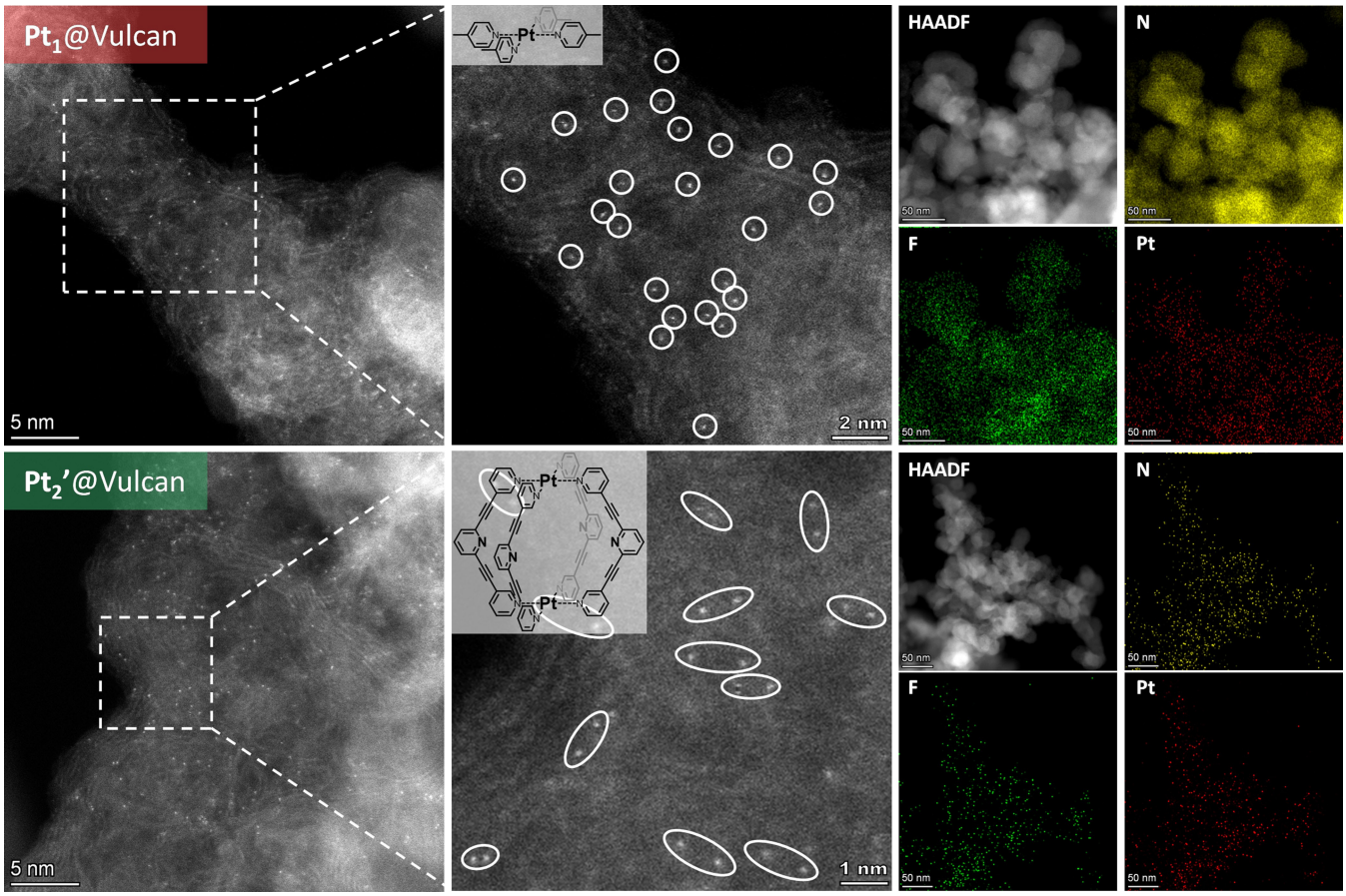

Figure 2. Structural characterization of **Pt$_1$**@Vulcan and **Pt$_2$'**@Vulcan. Aberration corrected HAADF-STEM imaging and energy-dispersive X-ray spectroscopy (EDX) of **Pt$_1$**@Vulcan (top) and **Pt$_2$'**@Vulcan (bottom). Spatially isolated Pt atoms and atomic pairs are indicated by the white circles and ovals, respectively.

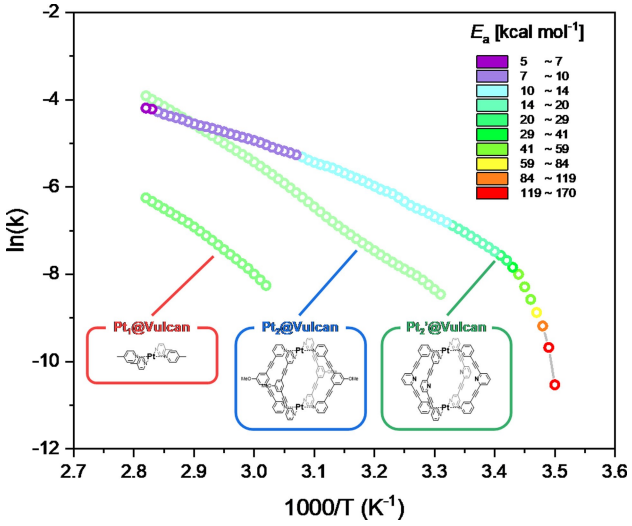

Figure 3. Arrhenius plots of **Pt$_1$**@Vulcan, **Pt$_2$**@Vulcan and **Pt$_2$'**@Vulcan in the hydrolysis of ammonia borane. Each data point represents a window average of 60 individual measurements. All experiments were performed in triplo from three different batches and the data shown here represent the averaged values.

We used ammonia borane hydrolysis as a probe reaction in our studies for a number of reasons. First, it produces significant amounts of hydrogen gas using little catalyst and its background reaction (using only Vulcan) is negligible. Moreover, we can study this gas evolution with high precision using our home-built automated bubble counter.[14] This simple and inexpensive device can run experiments under a temperature ramp, generating highly precise Arrhenius curves based on thousands of measurements enabling us to study subtle physico-chemical changes. Both ammonia borane and water can form hydrogen bonds with the pyridine groups in the second coordination sphere of **Pt$_2$'**. This allows us thus to evaluate how tailoring of the second coordination sphere around the platinum nodes can influence the reaction kinetics. The fact that two substrates need to be activated for a successful reaction makes this reaction highly sensitive to the structure and surroundings of the active site, making it an ideal probe reaction too.[15]

The catalysts were well-dispersed in water and the sample was cooled to 5 °C. Then, the reaction mixture was placed in the bubble counter device, ammonia borane was introduced and a temperature ramp of 2 °C min^{-1} was applied achieving a controlled temperature increase between 15 and 80 °C. The rate of ammonia borane hydrolysis was followed by quantifying the

amount of hydrogen gas evolved from the reaction mixture (Figure S33). The rate data is shown using the Arrhenius plot (Figure 3). For **Pt$_1$**@Vulcan and **Pt$_2$**@Vulcan only data at higher temperatures is depicted when comparing to **Pt$_2$'**@Vulcan. This is because these two catalysts do not catalyse the reaction sufficiently to have reliable data in this lower temperature regime.

Pt$_1$@Vulcan shows a classic Arrhenius behaviour and an activation energy of 21 kcal mol^{-1} (Figure 3). Additional isothermal experiments show that the rate of **Pt$_1$**@Vulcan is unaffected by ammonia borane concentration meaning that this reaction follows zero-order kinetics (Figure S34). This is generally observed for ammonia borane hydrolysis on supported single-metal-site catalysts and supported nanoparticles and implies that the O–H cleavage of water is the rate-determining step.[15]

While **Pt$_2$**@Vulcan also shows a classic Arrhenius behaviour and having a similar activation energy of 18 kcal mol^{-1}, its reaction rate is ten times higher compared to **Pt$_1$**@Vulcan (Figure 3 and Figure S33). In contrast to **Pt$_1$**@Vulcan and what is usually reported in literature, **Pt$_2$**@Vulcan shows a clear first-order rate dependence on ammonia borane concentration (Figure S35). This means that O–H cleavage is no longer the (only) rate-determining step and that ammonia borane is involved in the rate-determining step too. This suggests that the rate enhancement of **Pt$_2$**@Vulcan is caused by confinement effects of the cage-type structure. The confinement increases the *local* concentration of water close to the catalytically active Pt-N$_4$ site, facilitating O–H cleavage of water.

Next, we compared the catalytic performance of **Pt$_2$'**@Vulcan and **Pt$_2$**@Vulcan to learn how the proximity of pyridine functional groups in the second coordination sphere affects catalysis. Analogues to **Pt$_2$**@Vulcan, **Pt$_2$'**@Vulcan also shows a first-order rate dependence on ammonia borane concentration (Figure S36). An interesting difference between the two catalysts was noted in how the rate responds to temperature: the Arrhenius plot for **Pt$_2$'**@Vulcan is curved (Figure 3) while that of **Pt$_2$**@Vulcan is straight. This curved plot of **Pt$_2$'**@Vulcan indicates that E_a is continuously changing with temperature, decreasing from 166 to 5 kcal mol^{-1} as the temperature increases from 15 to 80 °C. Most of the curvature of the **Pt$_2$'**@Vulcan plot is at temperatures where **Pt$_2$**@Vulcan is not sufficiently active for reliable data. However, comparing the two from 30 to 80 °C, we see that **Pt$_2$'**@Vulcan still shows significant curvature, with E_a decreasing from 15 to 5 kcal mol^{-1}. Such change in the slope of the Arrhenius plot usually reflects either a different reaction mechanism and/or a physical change in the system. As we see here a gradual change rather than a clear inflection point, a different mechanism is unlikely.[16] A physical change of the catalyst itself is also unlikely as a stability test running for 15 h at 65 °C showed no deactivation, giving a TON of 36,000 (Figure S40).

Mechanistic studies

As **Pt$_2$**@Vulcan shows no curvature in its Arrhenius plot, the curvature in the plot of **Pt$_2$'**@Vulcan must be caused by the pyridine groups that points towards the inside of the cage cavity (Figure 3). These functional groups could enhance the binding of the rate limiting substrate ammonia borane by their lone pair on nitrogen, but NMR titrations show that this binding is weak (Figures S42–S43). However, further binding studies by HR-ESI-MS showed the cage-NH_3BH_3 adduct for **Pt$_2$'** but not for **Pt$_2$**, indicating weak binding of ammonia borane in **Pt$_2$'** (Figures S44–S45). Thus, by tailoring the catalyst' second coordination sphere, the *local* concentrations near the platinum nodes may be increased explaining the enhanced activity at lower temperatures.

Additionally, the pyridine could act here as a base, abstracting a proton from water (Eq. 2).

$$C_6H_5N + H_2O \leftrightarrow C_6H_5NH^+ + OH^- \quad (2)$$

Such an equilibrium shifts to the right with increasing temperature.[17] This would explain the curvature in the Arrhenius plot as the OH^- promotes the hydrolysis of ammonia borane by stabilizing the transition state.[18] Thus, the reduced E_a at higher temperatures may also reflect a higher *local* OH^- concentration. Overall, our data implies that inserting pyridine functional groups in the secondary coordination sphere can lower E_a by substrate pre-organization and/or transition state stabilization. The resulting E_a is only 5 kcal mol^{-1} at 80 °C for **Pt$_2$'**@Vulcan (Figure 3), indicating diffusion-controlled kinetics.

To gain further insight into the reaction mechanism, we ran deuterium-labelled experiments using D_2O and NH_3BD_3 and determined the respective kinetic isotope effect (KIE) values (Figure 4).

Importantly, we see that using these deuterated substrates the reaction remains first-order in ammonia borane. Thus, the reaction mechanism itself is unchanged by deuterium substitution and the KIE values provide insight in the original mechanism. Taking the initial rate of both reactions and comparing it with the reaction using non-deuterated substrates yielded a KIE of 1.7 in both cases. To exclude the possibility that the values are identical because of H–D exchange between ammonia borane and water, additional scrambling studies were performed. Solutions of NH_3BH_3 in D_2O and NH_3BD_3 in H_2O were

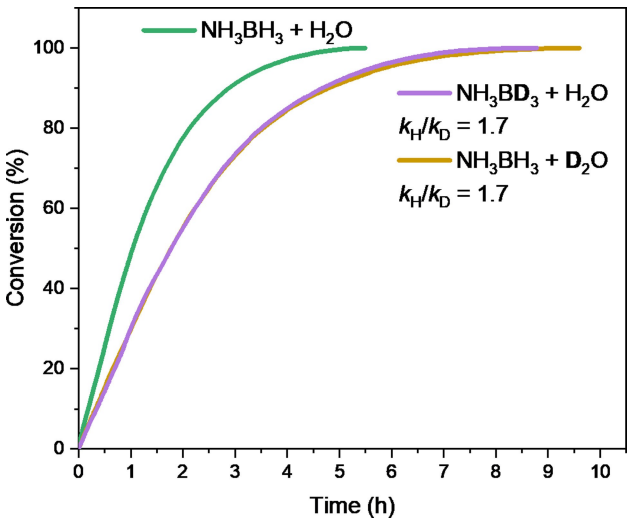

Figure 4. Kinetic isotope studies of **Pt$_2$'**@Vulcan in the hydrolysis of ammonia borane.

heated to 65 °C and analysed by ^{11}B-NMR confirming the absence of H–D exchange under these conditions (Figure S41). As the KIE values are identical, we suggest that both substrates are activated in the same concerted rate-determining step, where one of the B–H bonds of ammonia borane and the O–H bond of water is broken and new B–O and H–H bonds are formed. The relatively low magnitude of the KIEs supports such a bent transition state, as hydrogen transfer through bent transition states often give low primary KIEs.[19]

Conclusions

Surface immobilization of supramolecular cages is a powerful method for synthesizing supported single-metal-site catalysts with well-defined primary and secondary coordination spheres. Using high-precision kinetic studies at various temperatures, we show how the secondary coordination sphere can increase reaction rates and lower activation barriers. This understanding helps us to tailor the reaction pocket to achieve near-perfect kinetics, reducing the energy of activation to the diffusional regime. We show the importance of careful design of the active site's surroundings, and provide a versatile strategy for doing this.

Experimental Section

General Considerations. All reactions were carried out in air at room temperature unless noted otherwise. To prevent cross-contamination of trace metals, all glassware used were single use scintillation vials or glassware which was cleaned with aqua regia (HNO_3:HCl 1:3 molar ratio) before use. All water used was demineralized water which was deionized by the Milli-Q technique and has a resistance greater than 18.2 MΩ cm at room temperature. Diethyl ether and pentane were distilled from sodium under a N_2 atmosphere and used directly from the distillation setup. All reagents were purchased from commercial suppliers and used without further purification unless mentioned otherwise. Specifically, ammonia borane (technical grade, 90%) and D_2O (99.9 atom% D) were obtained from Sigma Aldrich, Vulcan XC72 was obtained from Cabot, acetonitrile (99.9%, Extra Dry over Molecular Sieve, AcroSeal) was obtained from Fisher Scientific B.V and ammonia borane-d_3 (NH_3BD_3) was synthesized according to the procedure of Gagare and co-workers using $NaBD_4$ instead of $NaBH_4$.[20] The self-assembled supramolecular structures $Pt_1L_4(BF_4)_2$ (**Pt_1**, L = *p*-picoline),[11] $Pt_2L_4(BF_4)_4$ (**Pt_2**, L = 3,3′-((5-methoxy-1,3-phenylene)bis(ethyne-2,1-diyl))dipyridine)[11] and $Pt_2L'_4(BF_4)_4$ (**Pt_2′**, L = 2,6-bis(pyridine-3-ylethynyl)pyridine)[10] were synthesized according to literature procedures. **Pt_1** was stored as a solid while **Pt_2** and **Pt_2′** were stored as solutions (2.5 mM) in MeCN in J Young Schlenk flasks at 5 °C. ^{1}H-NMR and DOSY-NMR, ^{13}C-NMR and HR-ESI-MS results were in agreement with the published data confirming the clean formation of the desired supramolecular constructs (Figures S1–S15).

Instrumentation and characterization methods. ^{1}H- and ^{13}C-NMR spectra were recorded on a Bruker AVANCE III HD 300 MHz spectrometer at room temperature and referenced to the solvent residual signal (1.94 ppm for CD_3CN) and converted to the TMS scale. The following abbreviations are used in reporting the NMR data: s (singlet), d (doublet), dd (doublet of doublets) and dt (doublet of triplets). Spectra interpretations are reported as follows: chemical shift (corresponding nucleus, multiplicity, coupling constant(s), integration). Data was processed and visualized using MestReNova 10.0.2.

2D ^{1}H-Diffusion ordered spectroscopy (DOSY) spectra were recorded on a Bruker AVANCE III HD 300 MHz spectrometer at a controlled temperature of 25.0 °C in CD_3CN and referenced to the solvent residual signal (1.94 ppm for CD_3CN at log D = −8.38 m^2s^{-1}).[21] Before each DOSY measurement, both the temperature and the magnetic gradient were calibrated first. Data fitting and visualization was performed by Bruker TopSpin 4.1.1. The hydrodynamic radii of the organometallic species were estimated based on their diffusion constants using the Stokes-Einstein equation (Eq. 3).

$$D = \frac{k_b \times T}{6\pi \times \eta \times r} \quad (3)$$

In which D = diffusion coefficient in m^2s^{-1}, k_b = Boltzmann constant = 1.38×10^{-23} N m K^{-1}, T = temperature in Kelvin, η = viscosity of the used solvent in N m^{-2} s and r = radius in m.

Mass spectra were collected on a HR-ToF Bruker Daltonik GmbH (Bremen, Germany) Impact II, an ESI-ToF MS capable of resolution of at least 40000 FWHM. Detection was in positive-ion mode and the source voltage was between 4 and 6 kV. The sample was introduced with a syringe pump at a flow rate of 180 μl*hr^{-1}. The drying gas (N_2) was held at 35 °C and the spray gas was held at 60 °C The machine was calibrated prior to every experiment via direct infusion of a TFA–Na solution, which provide a m/z range of singly charged peaks up to 3500 Da in both ion modes. Data acquisition was performed by Bruker Compass 2.0.

UV-Vis spectra were obtained on a double beam Shimadzu UV-2600 spectrometer at room temperature using quartz cuvettes with a path length of 2 or 10 mm and clean solvent as a background. Spectra were obtained between 200 and 800 nm using a spectral bandwidth of 0.5 nm. After data acquisition, the spectra were zeroed at 800 nm.

Single crystal X-ray diffraction (sc-XRD) data of **Pt_1** and **Pt_2′** was acquired on a Bruker D8 Quest Eco diffractometer using graphite-monochromated (Triumph) Mo Ka radiation (l = 0.71073 Å) and a CPAD Photon III C14 detector. Crystals suitable for single crystal X-ray diffraction of **Pt_1** were grown by vapor diffusion of tetrahydropyran in a solution of **Pt_1** in acetonitrile at room temperature over the course of seven days and for **Pt_2** by vapor diffusion of diisopropyl ether (iPr_2O) in a solution of **Pt_2** in acetonitrile at room temperature over the course of 2 days. The samples were cooled with N_2 to 100 K with a Cryostream 700 (Oxford Cryosystems). Intensity data were integrated using the Bruker *SAINT* software, V8.40B, Bruker *AXS* Inc., Madison, Wisconsin, USA, 2001. Absorption correction and scaling was executed with SADABS.[22] The structures were solved using intrinsic phasing with the program SHELXT 2018/2 against F^2 of all reflections.[23] Least-squares refinement was performed with SHELXL-2018/3.[24] All non-hydrogen atoms were refined with anisotropic displacement parameters. The hydrogen atoms were introduced at calculated positions with a riding model. The pyridine-functionalized cage **Pt_2′** crystallized in the tetragonal space group I4/m (a = b = 10.9330(7) Å, c = 35.653(4) Å). The crystal structure of **Pt_2′** contained a large void (total solvent accessible volume = 1406 $Å^3$, 567 e^-), containing highly disordered BF_4^- counterions and residual solvents, CH_3CN and iPr_2O, within the asymmetric unit that could not be refined reliably. Thus, the SQUEEZE procedure in PLATON (Version 301021)[25] was applied, accounting for 567 electrons per unit cell, congruent with the presence of 4×BF_4^- (40 e^-/molecule), 2×CH_3CN (22 e^-/molecule)

and 6×iPr_2O (58 e^-/molecule) solvent molecules in the unit cell. Deposition Numbers **2256149** (for **Pt_1**), **2255852** (for **Pt_2'**) contain the supplementary crystallographic data for this paper. These data are provided free of charge by the joint Cambridge Crystallographic Data Centre and Fachinformationszentrum Karlsruhe Access Structures service.

Powder X-Ray diffraction (pXRD) patterns were obtained with a Rigaku MiniFlex II diffractometer (Tokyo, Japan) using Ni-filtered CuKα radiation (λ = 1.541874 Å) at 30 kV and 15 mA. For each measurement, the sample was ground and loaded on a monocrystalline silicon sample holder with an 8 mm wide and 0.2 mm deep cavity. The powdered sample was pressed firmly in the cavity to make a uniform flat sample area. Residual sample outside the sample cavity was removed to minimize background scattering. Diffraction patterns were collected between the 2θ range of 5° and 80° using a rotation speed of 2° min^{-1}, a step size of 0.05° and 1 s dwell time.

Metal loadings were determined based on Inductively coupled plasma optical emission spectrometry (ICP-OES) analysis performed by the Mikroanalytisches Laboratorium Kolbe, Oberhausen, Germany. Samples were prepared using microwave digestion and then analysed with a Spectro Arcos analyzer of Spectro capable of maintaining a standard error of ± 1.5 ppm.

X-ray photoelectron spectroscopy (XPS) was performed on two different setups. The data of the immobilized catalysts was acquired using a Scienta Omicron HiPP-3 analyzer operated in Swift Acceleration mode and a monochromatic Al Kα source operating at 20 mA emission current. The base pressure was about 2×10^{-9} mbar, and the operating pressure was about 5×10^{-9} mbar. Survey and high-resolution spectra were acquired at pass energies of 500 eV and 300 eV respectively. XPS data of the organometallic species was performed on a Thermo Fisher ESCALAB 250Xi equipped with a monochromatic Mg X-ray source (Mg Kα = 1253.6 eV). XPS spectra were acquired in the standard lens mode using a concentric hemispherical analyzer and the mode of analyzer operation was the constant analyzer energy (CAE) mode. Survey spectra were obtained with a step size of 1.0 eV over two scans at a pass energy of 100.0 eV and high-resolution spectra were obtained with a step size of 0.05 eV over five scans with a pass energy of 30.0 eV. Prior to any data processing, the binding energies were calibrated using that of C 1s (284.8 eV). XPS peak fitting was performed using KolXPD software from Kolibrik, employing a Shirley background and Voigt functions for the individual components.

Aberration-corrected high angle annular dark-field scanning transmission electron microscopy (AC-HAADF-STEM) measurements, elemental mappings, and energy-dispersive X-ray spectroscopy (EDS) measurements were taken on a ThermoFisher Scientific FEI Themis Z instrument coupled with a high-angle annular dark field (HAADF) detector and an energy-dispersive X-ray spectroscopy detector. The samples were deposited on a Holey carbon coated TEM-grid (300 mesh Cu grid, Pacific Grid Tech, USA). The set-up was operated at 200 kV and delivers a spatial resolution of ≤ 70 pm in both TEM and STEM resulting in atomic-resolution imaging of the samples. Intensity profiles were obtained by using the Gwyddion 2.61 software package.

Cage precipitation. For pXRD analysis, **Pt_2** and **Pt_2'** were obtained as solids by the following precipitation procedure. Cage solutions in acetonitrile (3 mL, 2.5 mM) were added to a vigorously stirring solution of diethyl ether (20 mL) resulting in the formation of an off-white precipitate in a colourless solution. Then, pentane (20 mL) was added resulting in more precipitation and the reaction mixture was stirred vigorously for one hour. After precipitation, the reaction mixture was centrifuged (4000 rpm for 5 minutes) resulting in a white residue and a colorless supernatant. The supernatant was decanted and replaced by fresh diethyl ether (25 mL). Thereafter, the purified specimen was resuspended by ultrasonication for fifteen minutes. Subsequent centrifugation (4000 rpm for 5 minutes) and decantation of the supernatant yielded the desired cages structures in the solid form as white powders with an average yield of 90%.

Surface immobilization. The self-assembled supramolecular structures **Pt_1**, **Pt_2** and **Pt_2'** were immobilized on the heterogeneous support Vulcan XC72 by a conventional wet impregnation method. Vulcan XC72 (1.00 gram) was finely dispersed as a black suspension in acetonitrile (60 mL) by ultrasonication in a 250 mL round bottom flask for one hour. Then, an acetonitrile solution of the respective organometallic complex (10 mL, 0.5 mM Pt, 5.0 μmol Pt) was added dropwise to the Vulcan XC72 suspension over the course of three hours under vigorous stirring. After complete addition, the reaction mixture was left to stir at room temperature for an additional sixteen hours. Thereafter, acetonitrile was removed *in vacuo* over the course of one hour. The remaining black powder was further dried under vacuum (5 mbar at 50 °C) for sixteen hours and named **Pt_1**@Vulcan, **Pt_2**@Vulcan and **Pt_2'**@Vulcan, respectively.

Catalyst desorption and characterization. The immobilized catalysts (40 mg) were finely dispersed as a black suspension in DMSO (1 mL) by ultrasonication in a 4 mL screwcap vial for one hour. Thereafter, the reaction mixture was centrifuged (4000 rpm for 5 minutes) resulting in a black residue and a slightly yellow supernatant. The supernatant was subsequently analyzed by UV-Vis spectroscopy and HR-ESI-MS to quantify the amount (UV-Vis) of desorbed material and to confirm its structure (HR-ESI-MS).

Kinetic studies of ammonia borane hydrolysis. Reaction kinetics of ammonia borane hydrolysis were studied using a homebuilt bubble counter of which the design[14] and data processing[15] is described in detail elsewhere. Briefly, after a stirring catalyst solution was at the desired temperature, the reactor was closed off and an aqueous ammonia borane solution was directly injected into the reaction mixture causing a small volume displacement. This, and any further gas evolution caused by the hydrolysis of ammonia borane forming hydrogen gas was detected by analysing bubble formation from a hexadecane medium. Bubbles were detected with the aid of a laser and translated into an evolved volume of gas. Corrections for gas expansion of the head space of the reactor and increased vapor pressure of the used solvent at elevated temperatures were made and corrected for in all experiments.

For non-isothermal ammonia borane hydrolysis, a screwcap vial (10.0 mL) was charged with a stirring bean (8.0×3.0 mm), catalyst (40.0 mg) and water (8.0 mL). The catalyst was homogeneously suspended with the aid of an ultrasonic bath for ten minutes at room temperature. The screwcap vial was mounted on the reactor head. A freshly prepared ammonia borane solution (0.4 mL, 2.0 M) was loaded into syringe (1.0 mL) equipped with a glass capillary (Ø = 0.32 mm, l = 15 cm). The capillary was inserted through one of the syringe ports into the reaction mixture and purged with nitrogen (5.0 mL min^{-1}) while the reaction mixture was cooled down to 5.0 °C by an external ice bath. When this temperature was reached, the reactor was placed in the heating mantle under stirring and the other three remaining syringe ports were closed off. After five seconds, the ammonia borane solution was injected and a ramp of 2.0 °C min^{-1} was initiated. The sample was heated to 80.0 °C and held there until no gas production was observed anymore.

For isothermal ammonia borane hydrolysis, a screwcap vial (10.0 mL) was charged with a stirring bean (8.0×3.0 mm), catalyst (40.0 mg) and water (8.0 mL). The catalyst was homogeneously suspended with the aid of an ultrasonic bath for ten minutes at room temperature. The

screwcap vial was mounted on the reactor head. An ammonia borane solution (0.4 mL, 2.0 M) was loaded into syringe (1.0 mL) equipped with a glass capillary (Ø = 0.32 mm, l = 15 cm). The capillary was inserted through one of the syringe ports into the reaction mixture and purged with nitrogen (5.0 mL min^{-1}) while pre-heating the reaction mixture to 65.0 °C under stirring by the use of a heating mantle. When stabilized at 65.0 °C, the other three remaining syringe ports were closed off and the ammonia borane solution was injected. Gas production was monitored until reaction completion keeping the temperature of the reaction mixture at 65.0 °C.

For the stability tests, the reaction mixture is centrifuged (4000 rpm for 10 minutes) after reaction completion in its original screw cap vial (10.0 mL) resulting in a black residue and a colorless supernatant. The aqueous supernatant was removed with a needle and replaced by fresh water to a total volume of 8.0 mL. Thereafter, the purified specimen was resuspended by ultrasonication for fifteen minutes. This washing procedure was repeated three times before a subsequent catalytic reaction was started. After the last run, the aqueous supernatant was removed, and the remaining black powder was further dried under vacuum (5 mbar at 50 °C) for sixteen hours. Thereafter, the amount of remaining catalyst was weighed to determine any catalyst losses during the washing procedures, this loss was determined to be insignificant for all experiments.

For the kinetic isotope studies, these are performed identical to isothermal ammonia borane hydrolysis experiments, but then using D_2O or NH_3BD_3 instead. The rate constants are determined below 20% conversion by a linear fit to the reaction profile. The KIE value is determined by dividing the rate constants for the reaction involving hydrogen (k_H) over its deuterium analogue (k_D), i.e. KIE = k_H/k_D.

Supporting information

Detailed experimental procedures for the preparation of all compounds and their characterisation, single-crystal structures of the complexes, ICP-OES data, X-Ray diffraction patterns, X-ray photoelectron spectroscopy data, details of the kinetic studies and data analysis, and full data of the sorption and binding studies.

Author Contributions

P. C. M. L., G. R., J. N. H. R. and N. Y. conceived and guided the project. P. C. M. L. performed catalyst synthesis, characterization and reactivity studies. E. O. B. performed synthesis of the supramolecular structures. F. J. D. Z. helped guiding the project and performed SC-XRD measurements and data analysis. J. A. V. performed initial reactivity studies. A. T. and R. B. performed XPS measurements and data analysis. P. C. M. L. and G. R. wrote the manuscript with input from all authors.

Acknowledgements

We thank the Netherlands Organization for Scientific Research (NWO) for the grant "Mimicking nature in designing bi-atom heterogeneous catalyst" (grant VI.Vidi.192.045, to N.Y.) and E. Zuidinga for HR-ESI-MS measurements.

Conflict of Interests

The authors declare no conflict of interest.

Data Availability Statement

The data that support the findings of this study are available from the corresponding author upon reasonable request.

Keywords: catalysis · kinetics · metal-organic cages · second-coordination sphere effects · single-atom catalysis · structure-performance relationships · surface chemistry

[1] X.-F. Yang, A. Wang, B. Qiao, J. Li, J. Liu, T. Zhang, *Acc. Chem. Res.* **2013**, *46*, 1740–1748.
[2] X. Cui, W. Li, P. Ryabchuk, K. Junge, M. Beller, *Nat. Catal.* **2018**, *1*, 385–397.
[3] S. Ji, Y. Chen, X. Wang, Z. Zhang, D. Wang, Y. Li, *Chem. Rev.* **2020**, *120*, 11900–11955.
[4] M. Raynal, P. Ballester, A. Vidal-Ferran, P. W. N. M. van Leeuwen, *Chem. Soc. Rev.* **2014**, *43*, 1660–1733.
[5] M. Raynal, P. Ballester, A. Vidal-Ferran, P. W. N. M. van Leeuwen, *Chem. Soc. Rev.* **2014**, *43*, 1734–1787.
[6] T. S. Koblenz, J. Wassenaar, J. N. H. Reek, *Chem. Soc. Rev.* **2008**, *37*, 247–262.
[7] S. H. A. M. Leenders, R. Gramage-Doria, B. de Bruin, J. N. H. Reek, *Chem. Soc. Rev.* **2014**, *44*, 433–448.
[8] M. Otte, *Eur. J. Org. Chem.* **2023**, e202300012.
[9] L. Pirondini, F. Bertolini, B. Cantadori, F. Ugozzoli, C. Massera, E. Dalcanale, *Proc. Natl. Acad. Sci. USA* **2002**, *99*, 4911–4915.
[10] E. O. Bobylev, D. A. Poole III, B. de Bruin, J. N. H. Reek, *Chem. Sci.* **2021**, *12*, 7696–7705.
[11] E. O. Bobylev, J. Ruijter, D. A. Poole III, S. Mathew, B. de Bruin, J. N. H. Reek, *Angew. Chem. Int. Ed.* **2023**, *62*, e202218162.
[12] G. A. Zickler, B. Smarsly, N. Gierlinger, H. Peterlik, O. Paris, *Carbon* **2006**, *44*, 3239–3246.
[13] E. Clementi, D. L. Raimondi, W. P. Reinhardt, *J. Chem. Phys.* **1967**, *47*, 1300–1307.
[14] T. K. Slot, N. R. Shiju, G. Rothenberg, *Angew. Chem. Int. Ed.* **2019**, *58*, 17273–17276.
[15] T. K. Slot, N. Riley, N. R. Shiju, J. W. Medlin, G. Rothenberg, *Chem. Sci.* **2020**, *11*, 11024–11029.
[16] D. G. Truhlar, A. Kohen, *Proc. Natl. Acad. Sci. USA* **2001**, *98*, 848–851.
[17] I. R. Bellobono, P. Beltrame, *J. Chem. Soc. B* **1969**, *0*, 620–623.
[18] Y. Ge, X. Qin, A. Li, Y. Deng, L. Lin, M. Zhang, Q. Yu, S. Li, M. Peng, Y. Xu, X. Zhao, M. Xu, W. Zhou, S. Yao, D. Ma, *J. Am. Chem. Soc.* **2021**, *143*, 628–633.
[19] E. V. Anslyn, D. A. Dougherty, *Modern Physical Organic Chemistry*, University Science Books, Sausalito, CA, **2006**, 421–441.
[20] P. V. Ramachandran, P. D. Gagare, *Inorg. Chem.* **2007**, *46*, 7810–7817.
[21] M. Holz, X. Mao, D. Seiferling, A. Sacco, *J. Chem. Phys.* **1996**, *104*, 669–679.
[22] L. Krause, R. Herbst-Irmer, G. M. Sheldrick, D. Stalke, *J. Appl. Crystallogr.* **2015**, *48*, 3–10.
[23] G. M. Sheldrick, *Acta Crystallogr. Sect. A* **2015**, *71*, 3–8.
[24] G. M. Sheldrick, *Acta Crystallogr. C Struct. Chem.* **2015**, *71*, 3–8.
[25] A. L. Spek, *Acta Crystallogr. C Struct. Chem.* **2015**, *71*, 9–18.

Manuscript received: June 26, 2023
Version of record online: ■■, ■■

RESEARCH ARTICLE

Cage control: Surface immobilization of supramolecular cages gives control over the first- and second coordination spheres of heterogeneous catalysts, enabling diffusion-controlled reaction kinetics.

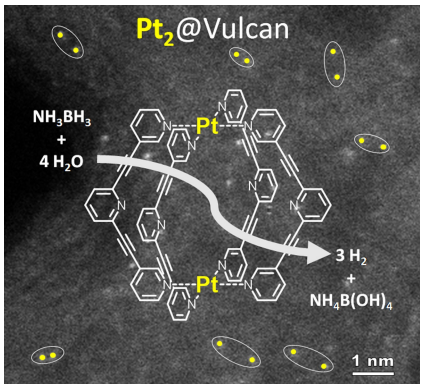

P. C. M. Laan, Dr. E. O. Bobylev, F. J. de Zwart, J. A. Vleer, A. Troglia, Dr. R. Bliem, Prof. Dr. G. Rothenberg, Prof. Dr. J. N. H. Reek*, Prof. Dr. N. Yan**